15-Copper(II)-containing 36-tungsto-4-silicates(IV) $[Cu_{15}O_2(OH)_{10}X(A\text{-}\alpha\text{-}SiW_9O_{34})_4]^{25-}$ (X = Cl, Br): synthesis, structure, magnetic properties, and electrocatalytic CO_2 reduction†

Bassem S. Bassil, [a,b] Ali Haider, [a,c] Masooma Ibrahim, [‡a] Ali S. Mougharbel, [a] Saurav Bhattacharya, [a] Jonathan H. Christian, [d] Jasleen K. Bindra, [d] Naresh S. Dalal, [d] Meng Wang,[e] Guangjin Zhang, [e] Bineta Keita,[f] Iwona A. Rutkowska, [g] Pawel J. Kulesza [g] and Ulrich Kortz [*a]

The 15-copper(II)-containing 36-tungsto-4-silicates $[Cu_{15}O_2(OH)_{10}X(A\text{-}\alpha\text{-}SiW_9O_{34})_4]^{25-}$ (X = Cl, **1**; Br, **2**) have been prepared in 70% yield by reaction of the trilacunary 9-tungstosilicate precursor $[A\text{-}\alpha\text{-}SiW_9O_{34}]^{10-}$ with Cu^{2+} ions in aqueous pH 8 medium. Both polyanions **1** and **2** were isolated as hydrated mixed potassium/sodium salts and characterized in the solid state by FT-IR, TGA, single-crystal XRD, and elemental analysis. DC magnetic susceptibility measurements from 1.8–300 K established the ground state to be paramagnetic with a magnetic moment corresponding to 15 uncoupled Cu^{2+} (S = 1/2) ions. EPR measurements and simulations were consistent with this analysis. Electrochemical studies were performed for polyanions **1** and **2** dissolved in solution to elucidate the electroactivity of both copper and tungstate sites. Using **2** as a representative example, the electrocatalytic activity towards CO_2 reduction upon deposition on a glassy carbon electrode surface, while retaining selectivity relative to hydrogen evolution, was demonstrated.

Introduction

Polyoxometalates (POMs) are discrete, anionic metal-oxides, and transition metal-containing heteropolytungstates represent a large subclass of POMs.[1] Due to the large number and structural as well as compositional versatility of lacunary POM precursors, which can act as inorganic multidentate ligands, there are numerous possibilities for generating new polyanions by incorporating one or more transition metal ions.[2] The class of copper(II)-containing POMs is of special interest for structural, magnetic, and catalytic reasons. In particular, Cu^{2+} as a $3d^9$ ion with a single unpaired electron represents an attractive center for electron paramagnetic resonance (EPR) studies.[3] A wide variety of copper(II)-containing POM structures has been reported to date. Classical 'sandwich'-type structures based on the so-called Weakley,[4] Hervé,[5] and Knoth[6] motifs are known. In addition, several other sandwich-type structures have been synthesized by using the dilacunary $[\gamma\text{-}XW_{10}O_{36}]^{8}$ (X = Si, Ge) POM precursors.[7] Also, the use of exogenous ligands, such as azide,[8] ammine,[9] carboxylate[10] and phosphonate[11] linkers, have been employed to form multi-copper(II)-containing POM structures with interesting physicochemical properties. A one-pot synthetic procedure based on reaction of salts of the composing elements is also known.[12] Our group has reported on $[Cu_5(OH)_4(H_2O)_2(A\text{-}\alpha\text{-}SiW_9O_{33})_2]^{10}$, with a pentacopper(II)-hydroxo fragment $\{Cu_5(OH)_4(H_2O)_2\}^{6+}$ being stabilized by two partially fused $[A\text{-}\alpha\text{-}SiW_9O_{34}]^{10}$ units.[13] Mialane's group reported $[Cu_{14}(OH)_{12}X(A\text{-}\alpha\text{-}SiW_9O_{34})_2(A\text{-}\alpha\text{-}SiW_9O_{33}(OH))_2]^{23}$, with a $\{Cu_{14}(OH)_{12}X\}^{15+}$ (X = Cl, Br) unit being stabilized by

[a]Jacobs University, Department of Life Sciences and Chemistry, Campus Ring 1, 28759 Bremen, Germany. E-mail: u.kortz@jacobs-university.de;
Fax: +49 421 200 3229; Tel: +49 421 200 3235
[b]Department of Chemistry, Faculty of Sciences, University of Balamand, P.O. Box 100, Tripoli, Lebanon
[c]Department of Chemistry, Quaid-i-Azam University, 45320-Islamabad, Pakistan
[d]Department of Chemistry and Biochemistry, Florida State University, Tallahassee, FL 32306-4390, USA
[e]CAS Key Laboratory of Green Process and Engineering, Chinese Academy of Sciences, 100190 Beijing, China
[f]Retired from Laboratoire de Chimie-Physique, UMR 8000 CNRS, Université Paris-Sud Orsay, F-91405, France
[g]Faculty of Chemistry, University of Warsaw, Pasteura 1, PL-02-093 Warsaw, Poland
‡Current address: Institute of Nanotechnology, Karlsruhe Institute of Technology (KIT), Hermann-von-Helmholtz Platz 1, 76344 Eggenstein-Leopoldshafen, Germany.

four trilacunary tungstosilicate(IV) units.[14] To date, the largest POM-stabilized copper(II) assembly is $[Cu_{20}X(OH)_{24}(H_2O)_{12}(P_8W_{48}O_{184})]^{25}$, with a 20-copper(II)-hydroxo cluster $\{Cu_{20}X(OH)_{24}(H_2O)_{12}\}^{15+}$ (X = Cl, Br, I) embedded in the wheel-shaped 48-tungsto-8-phosphate $[P_8W_{48}O_{184}]^{40}$.[15] Here we report on the facile synthesis and characterization of the 15-copper(II)-containing $[Cu_{15}O_2(OH)_{10}X(A\text{-}\alpha\text{-}SiW_9O_{34})_4]^{25}$ (X = Cl, **1**; Br, **2**) with a $\{Cu_{15}O_2(OH)_{10}X\}^{15+}$ assembly encapsulated by four $[A\text{-}\alpha\text{-}SiW_9O_{34}]^{10}$ units (see Fig. 1 and 2).

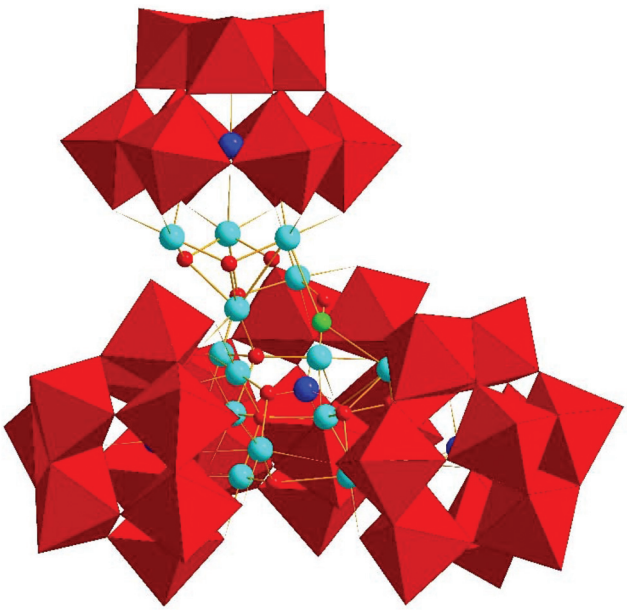

Fig. 1 Combined polyhedral/ball-and-stick representation of polyanions **1** and **2** (WO_6 red octahedral), Si blue, Cu turquoise, O red, Cl (1) and Br (2) light-green.

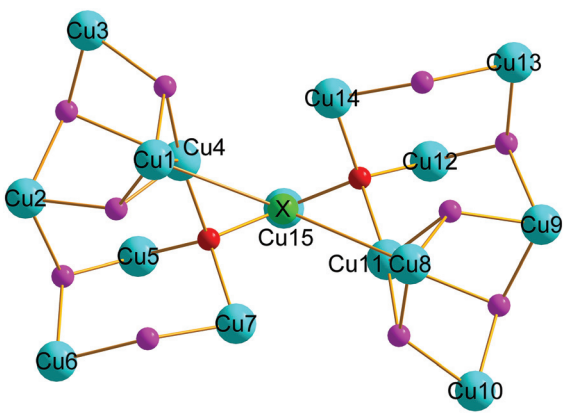

Fig. 2 View along the C_2 axis the $[Cu_{15}O_2(OH)_{10}X]^{15+}$ core assembly in **1** and **2**. The color code is the same as Fig. 1, with non-protonated oxygens in red and monoprotonated ones (hydroxide) in pink.

Experimental section

General notes

The $K_{10}[A\text{-}\alpha\text{-}SiW_9O_{34}]\cdot 24H_2O$ precursor for the synthesis of **KNa-1** was prepared according to the published procedure.[16] For the synthesis of **KNa-2** $K_{10}[A\text{-}\alpha\text{-}SiW_9O_{34}]\cdot 24H_2O$ was also used, but the latter was prepared with a slight modification. In order to avoid the presence of chloride ions during the synthesis of **2**, the $K_8\text{-}\alpha\text{-}[SiW_{11}O_{39}]\cdot 13H_2O$ precursor for the synthesis of $K_{10}[A\text{-}\alpha\text{-}SiW_9O_{34}]\cdot 24H_2O$ was washed with 6 mL saturated KBr solution instead of KCl.[17] Moreover, the crystalline $K_{10}[A\text{-}\alpha\text{-}SiW_9O_{34}]\cdot 24H_2O$ was washed with 10 mL of a saturated KBr (instead of KCl) solution.

The IR spectra were recorded on a Nicolet Avatar 370 FT-IR spectrophotometer using KBr pellets. The following abbreviations were used to assign the peak intensities: w = weak, m = medium, and s = strong. Elemental analysis was performed by Service Central d'Analyse, Solaize, France. Thermogravimetric analysis (TGA) was carried out on a TA Instruments SDT Q600 thermobalance with a 100 mL min^{-1} flow of nitrogen; the temperature was ramped from 25 to 600 °C at a rate of 5 °C min^{-1}.

Synthetic procedure

Synthesis of $Na_{3.5}K_{21.5}[Cu_{15}O_2(OH)_{10}(A\text{-}\alpha\text{-}SiW_9O_{34})_4Cl]\cdot 55H_2O$ (KNa-1). To a solution of $CuCl_2\cdot 2H_2O$ (0.11 g, 0.63 mmol) in 20 mL H_2O solid $K_{10}[A\text{-}\alpha\text{-}SiW_9O_{34}]\cdot 24H_2O$ (0.52 g, 0.20 mmol) was added upon stirring and after complete dissolution the pH of the clear green solution was raised to 8 by addition of 6 M NaOH solution. The solution was then stirred for one hour at room temperature. The turbid green solution was filtered and the filtrate was allowed to evaporate in an open vial at room temperature. The dark green crystalline product **KNa-1** started to appear on the next day and was collected by filtration after a week and air-dried. Yield: 0.420 g (70%). IR (2% KBr pellet, ν/cm $^{-1}$): 1005 (s), 942 (w), 909 (s), 802 (m), 752 (s), 665 (s), 526 (s) (see Fig. S1†). Elemental analysis (%) for **KNa-1**, calculated (found): Na 0.67 (0.62), K 7.00 (7.04), Cu 7.93 (7.89), Si 0.94 (0.90), W 55.1 (55.2), Cl 0.29 (0.20).

Synthesis of $Na_3K_{22}[Cu_{15}O_2(OH)_{10}(A\text{-}\alpha\text{-}SiW_9O_{34})_4Br]\cdot 60H_2O$ (KNa-2). This compound was synthesized following the same procedure as for **KNa-1**, but $K_{10}[A\text{-}\alpha\text{-}SiW_9O_{34}]\cdot 24H_2O$ washed with KBr solution (instead of KCl) was used as well as $CuSO_4\cdot 5H_2O$ as the copper(II) source. Moreover, 0.03 g of solid KBr was added to the solution before adjusting the pH to 8 with 6 M NaOH. Yield: 0.420 g (70%). IR (2% KBr pellet, ν/cm $^{-1}$): 1005 (s), 942 (w), 909 (s), 802 (m), 752 (s), 665 (s), 526 (s) (see Fig. S1†). Elemental analysis (%) for **KNa-2**, calculated (found): Na 0.57 (0.52), K 7.08 (7.01), Cu 7.84 (7.65), Si 0.92 (0.98), W 54.46 (53.67), Br 0.66 (0.72).

X-Ray crystallography

Single crystals were mounted on a Hampton cryoloop in light oil for data collection at 100 K. Indexing and data collection were performed on a Bruker D8 SMART APEX II CCD diffractometer with kappa geometry and Mo Kα radiation (graphite

monochromator, λ = 0.71073 Å). Data integration was performed using SAINT.[18] Routine Lorentz and polarization corrections were applied. Multiscan absorption corrections were performed using SADABS.[19] Direct methods (SHELXS97) successfully located the tungsten atoms, and successive Fourier syntheses (SHELXL14) revealed the remaining atoms.[20] Refinements were full matrix least-squares against $|F^2|$ using all data. In the final refinement, all nondisordered heavy atoms (W, Cu, Si, Cl, Br, K, Na) were refined anisotropically; oxygen atoms and disordered counter cations were refined isotropically. No hydrogen atoms were included in the models. For overall consistency we show in the CIF file the same formula unit as in the main text, with the exact numbers of counter cations and crystal waters (based on elemental analysis and TGA), as this reflects the true bulk composition of the compounds.

Crystal data for KNa-1. $ClCu_{15}H_{120}K_{21.50}Na_{3.50}O_{203}Si_4W_{36}$, M_W = 12009.58 g mol^{-1}; triclinic, space group $P\bar{1}$ a = 19.2429(6) Å, b = 20.9195(5) Å, c = 26.4944(8) Å, α = 106.8890(10)°, β = 101.894(2)°, γ = 90.921(2)°, V = 9953.4(5) Å^3, Z = 2, T = 173 K, D_c = 4.007 g cm^{-3}, 249 897 reflections collected, 33 575 unique (R(int) = 0.1058), R_1 = 0.0788, wR_2 = 0.2449.

Crystal data for KNa-2. $BrCu_{15}H_{130}K_{22}Na_3O_{208}Si_4W_{36}$, M_W = 12152.17 g mol^{-1}; triclinic, space group $P\bar{1}$; a = 19.239(2) Å, b = 20.836(2) Å, c = 26.480(3) Å, α = 106.806(5)°, β = 102.451(5)°, γ = 90.673(6)°, V = 9891.6(18) Å^3, Z = 2, T = 100 K, D_c = 4.080 g cm^{-3}, 307 418 reflections collected, 46 835 unique (R(int) = 0.0651), R_1 = 0.0985, wR_2 = 0.2157.

Crystallographic data are summarized in Table S1.† Further details on the crystal structures may be obtained from the Fachinformationszentrum Karlsruhe, 76344 Eggenstein-Leopoldshafen, Germany (Fax: (+49) 7247-808-666; E-mail: crysdata@fiz-karlsruhe.de), on quoting the depository numbers CSD – 433544 and 433545.†

Magnetic susceptibility measurements

Magnetic susceptibility (χ) measurements were carried out using a Quantum Design MPMS-XL SQUID magnetometer. Data for polycrystalline samples were collected over 1.8–300 K at 500 G, using a 38.37 mg sample. The data were corrected for the sample holder, and diamagnetism using Pascal constants.

EPR spectroscopy

Polycrystalline powder EPR spectra were recorded using a Bruker Elexsys-500 spectrometer at X-band (~9.5 GHz) and Q-band (~35 GHz) microwave frequencies in the 135–295 K temperature range. The magnetic field was calibrated using a DPPH standard (g = 2.0036). The modulation amplitude and microwave power were adjusted for optimal signal intensity and resolution in all measurements.

Electrochemistry

All reagents and chemicals were of high-purity grade and were used as purchased without further purification. The solutions were thoroughly deoxygenated for at least 30 min with pure argon and kept under a positive pressure of this gas during the experiments. The working electrode was well-cleaned ITO (0.3 cm^2). The electrochemical setup was a CHI workstation driven by a PC with the CHI660E software. A saturated calomel electrode (SCE) was used as reference in a compartment separated from the test solution by a fine porosity glass frit. Potentials during CO_2 electroreductions are quoted against the reversible hydrogen electrode (RHE). During the electrochemical measurements with POMs dissolved in solution, the counter electrode was a platinum plate with large surface area in a compartment separated from the test solution by a medium-porosity glass frit. The composition and pH of the supporting electrolyte were 1 M CH_3COOLi/CH_3COOH solution at pH 5. All experiments were performed at room temperature.

CO_2 reduction

Electrochemical measurements were performed using a CH Instruments Model 760D workstation (Austin, TX, USA) operating in three electrodes configuration. The glassy carbon working electrode was in the form of a disk with a geometric area of 0.071 cm^2. The reference electrode was a saturated calomel electrode (SCE: Hg, Hg_2Cl_2| KCl), and a carbon rod was set as the counter electrode. All diagnostic electrochemical measurements were performed in 0.1 mol dm^{-3} phosphate buffer of pH = 6.1 (obtained using potassium phosphate monobasic and potassium phosphate dibasic hydrates; from Sigma-Aldrich).

The catalytic inks were prepared by dissolution of 1.0 mg $Na_3K_{22}[Cu_{15}O_2(OH)_{10}(A\text{-}\alpha\text{-}SiW_9O_{34})_4Br]\cdot 60H_2O$ (**KNa-2**) in 100 μl water. Generally, 2 μl of the solution obtained were dropped onto the electrode surface. At the end, the film was covered by an ultrathin layer of Nafion polyelectrolyte by depositing 1 μl of the Nafion solution (prepared by diluting 5 mass% of the commercial Nafion solution into ethanol at 1 to 10 volume ratio).

All solutions were prepared using doubly-distilled and subsequently deionized (Millipore Milli-Q) water. They were deoxygenated by bubbling with high purity nitrogen for at least 30 min. During the electrocatalytic measurements, the electrolyte was saturated with CO_2 of premium quality (from Air Products) for at least 30 min the measurements were performed at room temperature (22 ± 2 °C).

Results and discussion

Synthesis and structure

The isostructural polyanions **1** and **2** were synthesized in good yield (70%) by reacting $CuCl_2\cdot 2H_2O$ and $CuSO_4\cdot 6H_2O$, respectively, with $K_{10}[A\text{-}\alpha\text{-}SiW_9O_{34}]\cdot 24H_2O$ in aqueous pH 8 medium at room temperature. The polyanions **1** and **2** crystallized as hydrated mixed potassium/sodium salts, $Na_{3.5}K_{21.5}[Cu_{15}O_2(OH)_{10}(A\text{-}\alpha\text{-}SiW_9O_{34})_4Cl]\cdot 55H_2O$ (**KNa-1**) and $Na_3K_{22}[Cu_{15}O_2(OH)_{10}(A\text{-}\alpha\text{-}SiW_9O_{34})_4Br]\cdot 60H_2O$ (**KNa-2**) in the space group $P\bar{1}$ with virtually identical cell parameters, rendering them isomorphous.

As expected, the FTIR spectra of **KNa-1** and **KNa-2** are essentially identical in the POM fingerprint region 400–1000 cm $^{-1}$ (Fig. S1†), which correspond to metal-oxo bending and stretching modes. Thermogravimetric analysis (TGA) was also performed on **KNa-1** and **KNa-2** (Fig. S2 and S3†) in order to estimate the number of crystal waters and to identify the thermal stability. Both compounds display a weight-loss step up to *ca.* 400 °C, which corresponds to loss of crystal waters as well as structural waters originating from protonated oxygens. The overall elemental composition of the bulk material was determined by complete elemental analysis.

Polyanions **1** and **2** have idealized C_2 point group symmetry and are hence chiral, but both enantiomers are present in equal amounts, resulting in the centrosymmetric space group $P\bar{1}$. The cationic $\{Cu_{15}O_2(OH)_{10}X\}^{15+}$ core unit (Fig. 2) comprises fifteen copper(II) ions, ten hydroxo- and two oxo-bridges as based on bond valence sum (BVS) calculations (see Table S2†).[21] This unit also has C_2 symmetry with the 2-fold axis passing through the halide ion and Cu15. The remaining 14 copper ions can be subdivided in seven pairs related by the 2-fold rotation axis, namely Cu1/Cu8, Cu2/Cu9, Cu3/Cu10, Cu4/Cu11, Cu5/Cu12, Cu6/Cu13, and Cu7/Cu14. The coordination environments of the copper(II) ions range from square-planar (Cu15), to square-pyramidal (Cu3/Cu10, Cu4/Cu11, Cu5/Cu12, Cu6/Cu13), to octahedral with Jahn–Teller distortion (Cu1/Cu8, Cu2/Cu9, Cu6/Cu13). The Cu1/Cu8 pair has the respective halido (Cl, **1**; Br, **2**) ligand *trans* to the axial oxo ligand. The ten hydroxo ligands include two μ_2- and eight μ_3-bridges, with the oxo ligand being a μ_4-bridge, as shown in Fig. 2. It is worth noting that the interatomic distance between Cu1 and Cu4 in **1** (2.854(5)) and **2** (2.848(3)) is rather short, which is expected to have a pronounced effect on their magnetic interaction (*vide infra*).

Polyanions **1** and **2** are closely related to Mialane's $[Cu_{14}(OH)_{12}X(SiW_9O_{34})_2(SiW_9O_{33}(OH))_2]^{23}$ (X = Cl, Br), which were synthesized from the azido-POM precursor $[(SiW_9O_{37})Cu_3N_3]^{11}$ when dissolved in aqueous NaCl and NaBr solutions respectively.[14] As shown in Fig. S4 and S5,† Mialane's and our structure differ mainly by the total number of copper(II) ions. The $\{Cu_{15}O_2(OH)_{10}X\}^{15+}$ core in 1 and 2 is very similar to Mialane's $\{Cu_{14}(OH)_{12}X\}^{15+}$ with an extra Cu^{2+} ion (Cu15) being embedded in the center and just below the halide bridge and alongside the C_2 axis. This copper-insertion results in a slight modification of the arrangement and protonation of the copper-hydroxo assembly. The two oxo-bridges of Cu14 become μ_4 and are no longer protonated, due to the insertion of a Cu^{2+} ion so that the chloro-bridge links the Cu1/Cu8 pair instead of Cu4/Cu11 (see Fig. S5†). Interestingly, due to the loss of exactly two protons accompanying the take-up of one Cu^{2+} ion, the $\{Cu_{15}\}$ core in **1** and **2** and Mialane's $\{Cu_{14}\}$ core have the exact same charge of 15^+.

Although the synthesis of **1** and **2** is rather simple (mixing of respective lacunary POM precursor and copper(II) salt followed by pH adjustment and stirring at room temperature) the reaction requires using the potassium salt of $[A\text{-}\alpha\text{-}SiW_9O_{34}]^{10}$. All attempts trying to synthesize **1** and **2** using the sodium salt of the POM precursor were unsuccessful. Differences in the reactivity of the sodium *vs.* potassium salts of $[A\text{-}\alpha\text{-}SiW_9O_{34}]^{10}$ have been noted previously.[16,22] Moreover, it is worth mentioning that polyanion **2** can only be prepared in a strictly chloride-free solution (suggesting that **1** is thermodynamically more stable than **2**). This can be achieved by preparing the $K_{10}[A\text{-}\alpha\text{-}SiW_9O_{34}]\cdot 24H_2O$ POM precursor in double-deionized water followed by bulk precipitation with KBr instead of KCl. In addition, $CuSO_4$ was used as a copper(II) source (instead of $CuCl_2$) and all the glassware was thoroughly washed with double-deionized water to avoid any chloride contamination. Interestingly, halide-free analogues of **1** and **2** could not be obtained, analogous to Mialane's $[Cu_{14}(OH)_{12}X(A\text{-}\alpha\text{-}SiW_9O_{34})_2(A\text{-}\alpha\text{-}SiW_9O_{33}(OH))_2]^{23}$ (X = Cl, Br),[14] and our $[Cu_{20}X(OH)_{24}(H_2O)_{12}(P_8W_{48}O_{184})]^{25}$ (X = Cl, Br, I).[15] Efforts to isolate the iodide-derivative of **1** and **2** were unsuccessful.

Magnetic properties

Magnetic susceptibility (χ) measurements were undertaken to establish the spin state of polyanions **1** and **2** in the solid state. Each Cu^{2+} ion has a $3d^9$ formal configuration with electronic spin $S = 1/2$. Fig. 3 (left) shows the measured effective magnetic moment (μ_{eff}) of **KNa-1** and **KNa-2** in units of Bohr magnetons from 1.8–300 K. Diamagnetic corrections of 3.20×10^{-3} and 3.221×10^{-3} emu mol^{-1} were calculated using Pascal constants and were added to the experimental data for **KNa-1** and **KNa-2**, respectively.[23] At room temperature, the magnetic moment of **KNa-1** is $6.25\mu_\beta$. A slightly lower moment of $5.19\mu_\beta$ was measured for **KNa-2**. For **KNa-1**, this value is close to the spin only value for 15 uncoupled $S = 1/2$ Cu^{2+} ions ($\mu_{eff} = 6.71\mu_\beta$) with $g = 2.0$ since χT of 15 uncoupled spins would be $15g^2S(S+1)/8$ and $\mu_{eff} = \sqrt{8\chi T}$. We tentatively ascribe the lower magnetic moment of **KNa-2** to the presence of diamagnetic impurities that could not be accounted for in our analysis. Both magnetic moments sharply decrease at lower temperatures, perhaps due to zero-field splitting or weak antiferromagnetic coupling. Normalized magnetization at 1.8 K between 0 and 6 T is shown in Fig. 3 (right). The magnetization does not saturate up to 7 T. These data were compared to Brillouin functions using $S = 1/2$, 1, and 3/2 (Fig. S7†). We found that the $S = 1/2$ Brillouin curve is in good agreement with our normalized magnetization data up to 6 T; a result

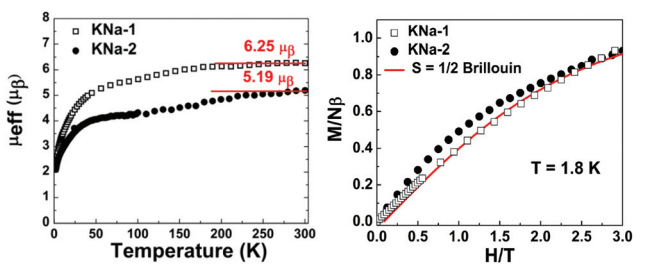

Fig. 3 (Left) Plot of μ_{eff} *vs.* T for **KNa-1** and **KNa-2**. (Right) Plot of magnetization *vs.* magnetic field for **KNa-1** and **KNa-2**.

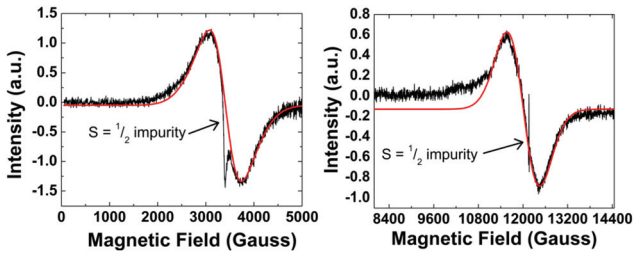

Fig. 4 Left: X-band EPR spectrum of **KNa-1** at 135 K (black) and the best fit simulation (red). Right: Q-band EPR spectrum of **KNa-1** at 135 K (black) and the best fit simulation (red).

that further supports our assertion that each Cu^{2+} ion has a $3d^9$ formal configuration with electronic spin $S = 1/2$.

X-band (~9.5 GHz) and Q-band (~35 GHz) electron paramagnetic resonance (EPR) between 135–295 K were used to further support our SQUID data analysis. Given the similarities in structure and SQUID measurements between **KNa-1** and **KNa-2**, we restrict our EPR analysis to **KNa-1** only. The 135 K X-band spectrum of **KNa-1** is shown in Fig. 4. The spectrum shows only a single peak at $g = 2.06 \pm 0.01$ with a peak-to-peak width of 710 ± 25 Gauss. Embedded within this peak is a sharp feature at $g \sim 2.01$ that we attribute to an unidentified radical impurity.

The slight asymmetry in the broad peak is attributed to the existence of an axially symmetric electronic environment. At 135 K and Q-band frequency, a single peak was again observed at $g \sim 2.06 \pm 0.02$ with a peak-to-peak width of 870 ± 25 Gauss. Again, embedded within the spectrum was a sharp impurity signal at $g \sim 2.01$. Both spectra were simulated using a locally developed program, as described elsewhere,[32] using the parameters of $S = \frac{1}{2}$ and $g_{\text{isotropic}} = 2.06$ with no hyperfine splitting. The lack of hyperfine or fine-structure is evidence of spin–lattice processes taking place between the ground state and low-lying excited state; as expected for this 15-spin cluster. These data confirm that the ground state is paramagnetic for both **KNa-1** and **KNa-2**, and are consistent with 15 uncoupled Cu^{2+} ions with more than one spin state located at energies close together and not resolvable by EPR spectroscopy.

Electrochemistry

In principle, the polyoxotungstate array in **1** and **2** has various accessible oxidation states, but effectively the reduction of W(VI) sites (*e.g.* to partially-reduced mixed-valence W(VI,V)-heteropolyblue, or more reduced W(VI,IV)-heteropolybrown structures) requires the availability of protons at the electrochemical interface.[24] As **1** and **2** are stable in neutral or semi-neutral (pH 6–7) media, the proton induced redox transitions are largely suppressed or diminished. On the other hand, the copper sites (existing within the polynuclear tungsten-oxo network) are expected to be electroactive and undergo reduction to Cu(0) in a manner analogous to Cu(I,II) oxides.

The results of conventional electrochemical measurements on the polyanions **1** and **2** dissolved in pH 5 acetate medium are illustrated in Fig. S8–S10.† The cyclic voltammetric (CV) responses of **1** and **2** are largely analogous, and they are consistent with previous reports on Cu^{II}-substituted POMs.[8c,15b] As expected, the CVs of both POMs reflect contributions from the redox processes (well-defined voltammetric peaks) related to the reduction of the Cu^{II} sites to Cu^0 *via* Cu^I (in the potential range from 0 to −0.8 V *vs.* SCE in Fig. S8 and S9†), followed by the partial reduction of W^{VI} centers at more negative potentials (Fig. S9†).

As featured in Fig. S8,† the CV behavior of the Cu^{II} centers in 1 consists of two reduction waves peaking at −0.242 V and −0.563 V (*vs.* SCE), respectively. By analogy to the earlier reports,[8c,15b] these voltammetric peaks shall be attributed to the stepwise reduction of the Cu^{II} centers to Cu^0 through the Cu^I state. In the reverse potential scan, a fairly large and narrow positive peak (typical for the oxidation or stripping of the deposited species from the electrode surface to the solution phase,[25] can be observed at about 0.1 V *vs.* SCE). When referring to the classical electrochemical behavior of copper (II, I, 0) species, the latter peak shall be attributed to the re-oxidation (to Cu^{II}) of Cu^0 deposited on the electrode surface during the negative (reduction) potential scans executed previously down to −0.8 V (*vs.* SCE). This result permits us to conclude that following reduction of the Cu^{II}-substituted POM (in solution at sufficiently negative potentials, *i.e.* around −0.6 V *vs.* SCE or lower), Cu^0 sites are generated most likely in the form of copper particles.[26–28] Reduction potential scans ending at less negative potentials (down to −0.3 V *vs.* SCE) result in the reversible formation of Cu^I sites; they can be readily reoxidized to Cu^{II} (black curve in Fig. S8†). Similar observations apply to the electrochemical behavior of **2** (Fig. S9†). Finally, upon application of potentials more negative than −0.8 V, the W^{VI} centers (both in **1** and **2**) can be partially reduced and, subsequently, reoxidized (Fig. S10†). The quasi-reversible pairs of voltammetric peaks observed here have similar shapes and comparable mid-peak potentials (−0.820 V and −0.826 V *vs.* SCE for **1** and **2**, respectively). This result reveals that the redox processes associated with the W^{VI} centers are not significantly influenced by the identity of the halide X.

CO_2 reduction

Regarding growing interest in the electrochemical conversion of carbon dioxide toward the production of useful chemicals (including alcohols, aldehydes and hydrocarbons),[29] and keeping in mind that copper, and particularly copper-oxide type systems, show the highest yields and efficiencies,[30] we have decided to probe here the electrocatalytic properties of **1** and **2** for CO_2-reduction. Furthermore, the presence of POM tungsten-oxo fragments at the electrocatalytic interface, and their ability to facilitate both mobility of protons and sorption of hydrogen,[25] should induce the CO_2-reduction while diminishing hydrogen evolution as the competitive process. Thus, under electrochemical (reduction) conditions, the system acts as a POM-based supramolecular-type assembly in which the

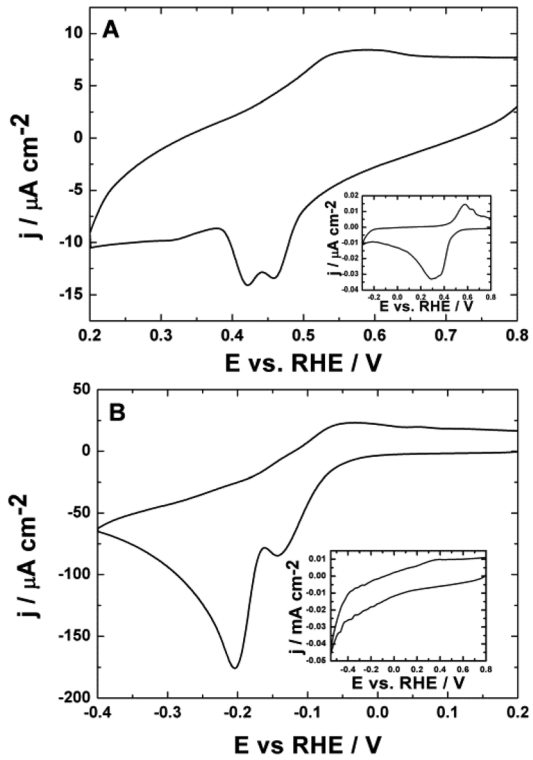

Fig. 5 Cyclic voltammetric response of **KNa-2** deposit on glassy carbon electrode, (B) $H_4SiW_{12}O_{40}{\cdot}xH_2O$ deposit introduced onto glassy carbon electrode modified with copper layer (obtained through electrodeposition by application of 0.3 V (*vs.* RHE) for 60 s in 5 mmol dm^{-3} $CuSO_4$ – 0.5 mol dm^{-3} H_2SO_4). Inset (A) illustrates the voltammetric behavior of **KNa-2** during potential cycling down to −0.3 V; the inset (B) shows the voltammetric characteristics of pristine $H_4SiW_{12}O_{40}$ on Cu-free glassy carbon electrode down to −0.55 V (*vs.* RHE) where hydrogen evolution starts to appear. Electrolyte: deoxygenated 0.1 mol dm^{-3} phosphate buffer (pH 6.1). Scan rate: 10 mV s^{-1}.

catalytic copper sites are precisely distributed within the high-surface-area hydroxyl-group-rich active tungsten-oxo matrix.

Diagnostic experiments aiming at addressing the electrocatalytic properties (CO_2-reduction) of **1** and **2** were performed under voltammetric conditions in phosphate buffer at pH 6.1 by using a glassy carbon electrode modified with **KNa-2** (Fig. 5A). A choice of this almost neutral (very weakly acidic) electrolyte was compromised by taking into account the reaction requirements (danger of the competition from hydrogen evolution) and the stability of the system.[26,29b] As common in the literature, the electrochemical data concerning CO_2-reduction (mechanisms are proton dependent) are expressed against the standard RHE electrode. By taking into account the actual potential of the SCE reference and the hypothetical change of pH from 6.1 to 0 (requirement for RHE standard), 0.602 V must be added to the values recorded *vs.* SCE to recalculate and consider them in the RHE scale.

The purpose of initial voltammetric experiments was to identify the copper electroactivity in **2** deposited on the electrode surface (in the absence of CO_2). Care was exercised to apply neither too negative nor too positive potentials, namely to avoid excessive hydrogen evolution or polyanion degradation. The reduction scan was started from the fairly positive potential of 0.8 V (*vs.* RHE) where the copper centers are in the oxidized (Cu^{2+}) state. At potentials lower than 0.5 V (*vs.* RHE), two-step reduction of Cu^{2+} sites occurred *via* Cu^{+} to Cu^{0}.[28] The actual voltammetric wave appearing in the range from 0.55 to 0.35 V (*vs.* RHE) was in a form of two overlapping peaks characteristic of the two redox processes mentioned above. Following the generation of Cu^0 sites, the reoxidation step resulted in a broad peak starting at about 0.45 V (*vs.* RHE) consistent with their oxidation to Cu^{2+} sites. High background currents could reflect some contribution from the redox activity of the POM tungsten atoms to the latter process. Indeed, when **KNa-2** (deposit) was subjected to potential cycling in the broader range of potentials, the exceptionally high (and fairly broad) reduction peak at about 0.3 V was observed during the second reduction scan performed down to −0.3 V (inset of Fig. 5A). Under such conditions, not only the Cu^0 sites were generated. Most likely, the high reduction currents reflected the copper-induced reduction of tungsten atoms within the **KNa-2** deposit. As the reoxidation currents (at *ca.* 0.5 V) are relatively much smaller, the reduction process was largely irreversible. Historically, the formation of heteropoly-"brown" species had been postulated following the irreversible reduction of heteropolytungstates at more negative potentials.[24a,b] Although no degradation (decomposition) of the **KNa-2** deposit was observed following consecutive long-term potential cycling (50 cycles), the system' s structural reorganization must have occurred. This problem will be the subject of future work.

Our hypothesis that copper sites strongly influence the electrochemical behavior of polytungstates has been verified in parallel diagnostic experiments in which the model Keggin-type $H_4SiW_{12}O_{40}$ has been deposited and investigated at bare and copper-modified glassy carbon electrode surfaces. In the latter case, depending on the applied potential, Cu^{II}, Cu^{I} or Cu^0 sites are formed, and they may interact with the tungsten units. While in the absence of copper, the redox transitions of $H_4SiW_{12}O_{40}$ (Inset to Fig. 5B) are poorly defined, yielding drawn-out waves overlapping the capacitive type currents (as expected for the behavior of polytungstates in a largely H^+-free solution at pH 6.1), the $Cu/H_4SiW_{12}O_{40}$ interface has produced two irreversible reduction peaks (Fig. 5B) at potentials where Cu^{II}/Cu^{I} and Cu^{I}/Cu^0 processes are operative, respectively.[29b,31] These peaks cannot be attributed solely to the copper redox transitions. The copper reoxidation peak (at 0.55 V) is relatively small (thus implying a small loading of copper at the interface), the two dominating reduction peaks must reflect a sizeable contribution from the irreversible reduction of tungsten centers of the POM. Once more, the electrogenerated Cu^{I} and Cu^0 sites seem to interact with W^{VI} and induce irreversible formation of heteropoly-"brown" type species postulated earlier and mentioned above.[24a,b]

Assuming that, at sufficiently negative potentials, **KNa-2** exists in the form of an irreversibly-reduced, structurally-reorganized deposit with Cu^0 sites, we have hence investigated

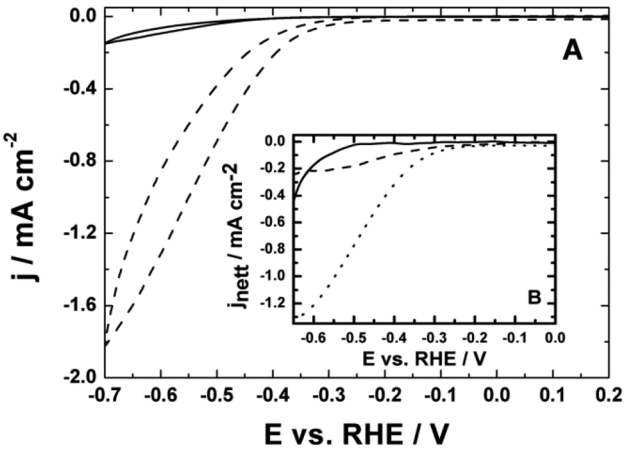

Fig. 6 (A) Cyclic voltammetric responses for **KNa-2** deposited on a glassy carbon electrode recorded in deoxygenated CO_2-free (solid line) and in CO_2-saturated (dashed line) 0.1 mol dm^{-3} phosphate buffer (pH 6.1). Scan rate: 10 mV s^{-1}. (B) Inset: Background-subtracted voltammetric currents for CO_2-reduction at **KNa-2** (dotted line), Cu_2O (dashed line), and $H_4SiW_{12}O_{40}$ (solid line) deposited on glassy carbon.

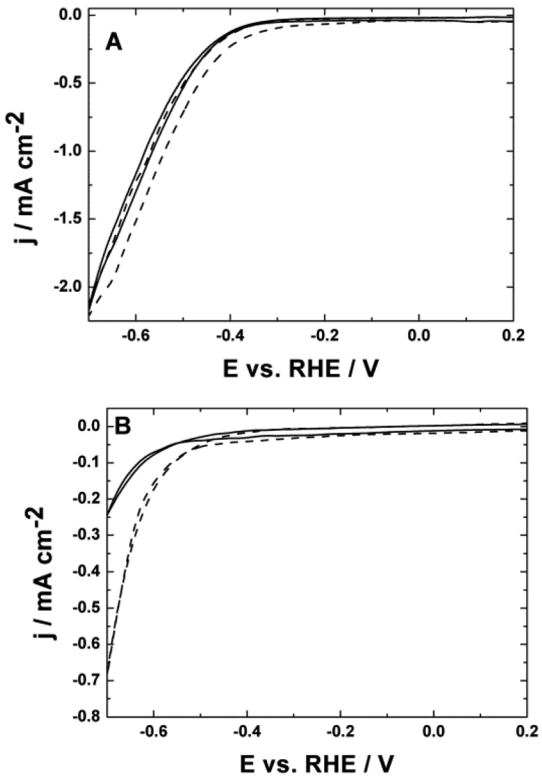

Fig. 7 Cyclic voltammetric characteristics of (A) Cu_2O nanoparticles and (B) $H_4SiW_{12}O_{40}$ (deposited on a glassy carbon disk) in the absence (solid line) and presence (dashed line) of carbon dioxide (saturated solution) in 0.1 mol dm^{-3} phosphate buffer (pH 6.1). Scan rate: 10 mV s^{-1}.

the activity of **KNa-2** toward the electroreduction of carbon dioxide (Fig. 6), an electrochemically inert and chemically very stable molecule. Fig. 6A illustrates voltammetric responses recorded both in the presence (dashed line) and the absence (solid line) of carbon dioxide. It should be noted that, contrary to the typical behavior of CO_2 at conventional copper electrodes, where hydrogen evolution is not only competitive but becomes also the predominant reaction hiding the CO_2 reduction (further complicated by the appearance of inhibiting CO intermediate adsorbates),[32] the present result is consistent with a high electrocatalytic selectivity and appreciable activity of **KNa-2** during the CO_2-elelctroreduction.[32] Simple comparison of currents at potentials lower than −0.5 V *vs.* RHE (Fig. 6) clearly implies that the CO_2 reduction currents are much larger here than those originating from hydrogen evolution.

Careful examination and comparison of the net (background-subtracted) CO_2-reduction currents (Fig. 6B, dotted line) recorded for **KNa-2**, relative to the analogous responses at "single component deposits", namely conventional Cu-free heteropolytungstate ($H_4SiW_{12}O_{40}$) and copper oxide (Cu_2O) investigated under the same experimental conditions, implies that both the reduced tungsten and copper components exhibit electrocatalytic activity toward the CO_2-reduction. Here Cu_2O, rather than simple copper, has been used because the reduced copper oxides are known to exhibit higher electrocatalytic activity toward CO_2-reduction.[30c] In order to gain insight in the simultaneous evolution of dihydrogen, which proceeds either through the reduction of protons ($2H^+ + 2e \rightarrow H_2$) or through reduction of water molecules ($2H_2O + 2e \rightarrow H_2 + 2OH^-$), we have considered here the responses both in the presence (dashed line) and absence (solid line) of CO_2 (Fig. 7). Contrary to the Cu_2O-based copper catalyst (Fig. 7A), where hydrogen evolution is the dominating reaction at potentials lower than −0.3 V (*vs.* RHE), the formation of H_2 at the Cu-free heteropolytungstate $H_4SiW_{12}O_{40}$ (Fig. 7B) is relatively suppressed (desired effect) and shifted toward more negative potentials (−0.5 V). In other words, the POM system seems to be more selective during the reduction of CO_2.

The data illustrated in Fig. 6 are consistent with the view that the coexistence of copper and tungsten sites in **2** results in the CO_2-reduction enhancement effect. Furthermore, it should be noted that the CO_2-reduction starts at potentials implying the predominant electrocatalytic activity of the copper sites (compare dashed lines in Fig. 6A and 7A), whereas the hydrogen evolution reaction is controlled, namely suppressed and shifted (compare solid lines in Fig. 6A and 7B) in a manner resembling performance of Cu-free heteropolytungstates. Although the present **KNa-2**-based electrocatalytic system has not been optimized in terms of the CO_2-reduction current densities (*e.g.* the preparation of deposits on electrodes with larger loadings of **KNa-2** would require the development of additional procedures for stabilization and immobilization), it is apparent from the data of Fig. 6 that the coexistence of copper and tungsten sites and their controlled distribution within **2** should lead to improved faradaic efficiency (suppressed H_2 evolution).

An enhanced activity of metallic Cu in the oxide environment was postulated earlier.[33] Partially reduced polyoxotung-

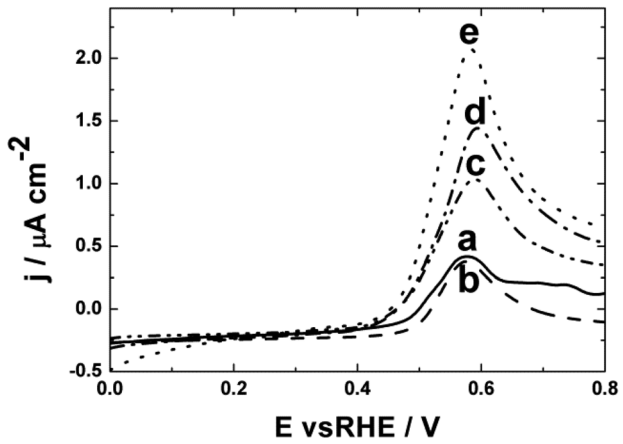

Fig. 8 Stripping-type (oxidation) voltammetric response of (a) the reaction (CO_2-reduction at −0.7 V) product adsorbate, recorded in comparison to the analogous responses of (b) formic acid, (c) acetaldehyde, (d) methanol, (e) ethanol considered as adsorbates in separate experiments in 0.1 mol dm^{-3} deoxygenated phosphate butter (pH 6.1). Scan rate: 10 mV s^{-1}.

states were reported to produce hydrogen-rich, highly-active "heteropoly-blue" and substoichiometric oxygen-deficient "heteropoly-brown" phases.[24a,b] By analogy to the performance of Pt in the presence of POMs,[24c] specific metal–oxide interactions between copper and tungsten-oxo species (*e.g.* alleviating CO poisoning) could also exist. Having in mind reaction pathways, they should also affect the binding energies of H and CO_2 related intermediates.

In order to comment on the nature of the reaction products after CO_2-electroreduction (as above), we have performed a series of diagnostic stripping-type voltammetric experiments (Fig. 8) in which the characteristic oxidation responses have been compared for the following adsorbates: (a) generated during CO_2-reduction (upon application of −0.7 V *vs.* RHE for 100 s) at the catalytic electrode (glassy carbon modified with **KNa-2**); relative to (b) formic acid, (c) acetaldehyde, (d) methanol, (e) ethanol (introduced onto the **KNa-2**-modified electrode surface upon dipping for 10 min in the external electrolyte solution containing the investigated system at 0.5 mol dm^{3} level). The fact that the potential for the oxidation of the CO_2-reduction product adsorbate (appearing at *ca.* 0.6 V *vs.* RHE) is almost identical to the oxidation potentials of other simple organic molecules implies that all of them, in addition to CO (appearing as the reaction intermediate during their oxidation) are possible reaction products of the electroreduction of CO_2 at **KNa-2**. This result is consistent with the existing literature describing the activity of Cu-based electrocatalysts.[31–34]

A combined electrochemical – mass spectrometric analytical study on pristine **KNa-2** was not possible due to insufficient stability of the POM during prolonged electrolysis. To perform some measurements, we stabilized the **KNa-2** deposit by soaking in an aqueous solution of 0.7 mmol dm^{3} 3,4-ethylenedioxythiophene/EDOT (Aldrich) monomer, followed by electropolymerization to PEDOT in an external phosphate buffer solution (10 potential cycles at 50 mV s^{1} from 0 to 1.2 V).[35] Information on the CO_2-reduction products was obtained by analyzing them after a long-term (2 h) electrochemical reduction of carbon dioxide (at −0.6 V *vs.* RHE; under conditions of Fig. 6). The experimental details of the approach had been described earlier.[36] The mass spectra obtained by using gas chromatography coupled with mass spectrometry (GC-MS) indicated the presence of ion peaks consistent with the presence of methanol and ethanol. While no carbon monoxide was identified at all potentials, the predominant contribution from H_2 evolution and the formation of low amounts (traces) of CH_4 and C_2H_4 was obvious at potentials more negative than −1.1 V (*vs.* RHE). The present GC-MS analytical data is preliminary and has only approximate meaning because the role of PEDOT is unclear and its presence may affect the electrocatalytic pathways.

Conclusions

In conclusion, we have synthesized the two 15-copper(II)-containing 36-tungsto-4-silicates **1** and **2** by one-pot reaction of the trilacunary POM precursor $[A\text{-}\alpha\text{-}SiW_9O_{34}]^{10}$ with the adequate Cu^{2+} salts. The novel polyanions were characterized in the solid state by FT-IR spectroscopy, single-crystal XRD, TGA and elemental analysis. Detailed magnetic susceptibility and EPR measurements show that the compounds are paramagnetic with a magnetic moment and EPR spectra corresponding to 15 uncoupled Cu^{2+} ($S = 1/2$) ions. The electrochemical behavior of both polyanions has also been addressed. A **KNa-2** deposit on an inert glassy carbon electrode exhibits electrocatalytic activity toward reduction of CO_2 in phosphate buffer (pH 6.1) while being largely selective against the competitive hydrogen evolution. Oxohydrocarbons, including ethanol and methanol, in addition to adsorbates of other oxygenated hydrocarbons, are among the possible reaction products.

Conflicts of interest

There are no conflicts to declare.

Acknowledgements

U. K. thanks the German Science Foundation (DFG-KO-2288/20-1) and Jacobs University for research support. P. J. K. and I. A. R. appreciate support from the National Science Center (Poland) under Maestro Project 2012/04/A/ST4/00287. We acknowledge CMST COST Action CM1203 (PoCheMoN). Fig. 1 and 2 were generated by Diamond, Version 3.2 (copyright Crystal Impact GbR).

Notes and references

1 (*a*) Topical issue on Polyoxometalates, *Chem. Rev*, ed. C. L. Hill, 1998, vol. 98, p. 1; (*b*) *Polyoxometalate Chemistry from Topology via Self-Assembly to Applications*, ed. M. T. Pope and A. Müller, Kluwer, Dordrecht, The Netherlands, 2001; (*c*) Y.-F. Song and R. Tsunashima, *Chem. Soc. Rev.*, 2012, **41**, 7384; (*d*) S.-T. Zheng and G.-Y. Yang, *Chem. Soc. Rev.*, 2012, **41**, 7623; (*e*) M. T. Pope and U. Kortz, Polyoxometalates, in *Encyclopedia of Inorganic and Bioinorganic Chemistry*, ed. R. A. Scott, John Wiley amp; Sons, Ltd, Hoboken, NJ, 2012; (*f*) ; Polyoxometalates, Cluster Issue, (U. Kortz and T. Liu, Guest Ed.), Eur. J. Inorg. Chem., 2013, pp. 7325–7648.

2 (*a*) G. S. Kim, H. D. Zeng, D. VanDerveer and C. L. Hill, *Angew. Chem., Int. Ed.*, 1999, **38**, 3205; (*b*) B. Godin, Y. Chen, J. Vaissermann, L. Ruhlmann, M. Verdaguer and P. Gouzerh, *Angew. Chem., Int. Ed.*, 2005, **44**, 3072; (*c*) A. Müller, M. T. Pope, A. M. Todea, H. Bögge, J. van Slageren, M. Dressel, P. Gouzerh, R. Thouvenot, B. Tsukerblat and A. Bell, *Angew. Chem., Int. Ed.*, 2007, **46**, 4477; (*d*) Q. Wu, Y. G. Li, Y. H. Wang, E. B. Wang, Z. M. Zhang and R. Clérac, *Inorg. Chem.*, 2009, **48**, 1606; (*e*) S.-T. Zheng and G.-Y. Yang, *Chem. Soc. Rev.*, 2012, **41**, 7623.

3 N. S. Dalal and C. A. Murillo, *Dalton Trans.*, 2014, **43**, 8565.

4 (*a*) T. J. R. Weakley and R. G. Finke, *Inorg. Chem.*, 1990, **29**, 1235; (*b*) U. Kortz, S. Isber, M. H. Dickman and D. Ravot, *Inorg. Chem.*, 2000, **39**, 2915; (*c*) L.-H. Bi, R.-D. Huang, J. Peng, E.-B. Wang, Y.-H. Wang and C.-W. Hua, *J. Chem. Soc., Dalton Trans.*, 2001, 121; (*d*) E. M. Limanski, M. Piepenbrink, E. Droste, K. Burgemeister and B. Krebs, *J. Cluster Sci.*, 2002, **13**, 369; (*e*) U. Kortz, S. Nellutla, A. C. Stowe, N. S. Dalal, U. Rauwald, W. Danquah and D. Ravot, *Inorg. Chem.*, 2004, **43**, 2308; (*f*) I. M. Mbomekalle, B. Keita, L. Nadjo, K. I. Hardcastle, C. L. Hill and T. M. Anderson, *Dalton Trans.*, 2004, 4094; (*g*) D. Drewes, E. M. Limanski and B. Krebs, *Eur. J. Inorg. Chem.*, 2005, 1542; (*h*) T. M. Anderson, X. Fang, I. M. Mbomekalle, B. Keita, L. Nadjo, K. I. Hardcastle, A. Farsidjani and C. L. Hill, *J. Cluster Sci.*, 2006, **17**, 183.

5 (*a*) F. Robert, M. Leyrie and G. Hervé, *Acta Crystallogr., Sect. B: Struct. Crystallogr. Cryst. Chem.*, 1982, **38**, 358; (*b*) P. Mialane, J. Marrot, E. Rivière, J. Nebout and G. Hervé, *Inorg. Chem.*, 2001, **40**, 44; (*c*) U. Kortz, N. K. Al-Kassem, M. G. Savelieff, N. A. Al Kadi and M. Sadakane, *Inorg. Chem.*, 2001, **40**, 4742; (*d*) U. Kortz, S. Nellutla, A. C. Stowe, N. S. Dalal, J. van Tol and B. S. Bassil, *Inorg. Chem.*, 2004, **43**, 144; (*e*) L.-H. Bi, B. Li, L.-X. Wu and Y.-Y. Bao, *Inorg. Chim. Acta*, 2009, **362**, 3309.

6 W. H. Knoth, P. J. Domaille and R. L. Harlow, *Inorg. Chem.*, 1986, **25**, 1577.

7 (*a*) H. Liu, C. J. Gómez-García, J. Peng, Y. Feng, Z. Su, J. Sha and L. Wang, *Inorg. Chem.*, 2007, **46**, 10041; (*b*) Z. Luo, P. Kögerler, R. Cao, I. Hakima and C. L. Hill, *Dalton Trans.*, 2008, 54; (*c*) Z. Luo, P. Kögerler, R. Cao and C. L. Hill, *Polyhedron*, 2009, **28**, 215; (*d*) N. H. Nsouli, A. H. Ismail, I. S. Helgadottir, M. H. Dickman, J. M. Clemente-Juan and U. Kortz, *Inorg. Chem.*, 2009, **48**, 5884.

8 (*a*) P. Mialane, A. Dolbecq, J. Marrot, E. Rivière and F. Sécheresse, *Chem. – Eur. J.*, 2005, **11**, 1771; (*b*) P. Mialane, C. Duboc, J. Marrot, E. Rivière, A. Dolbecq and F. Sécheresse, *Chem. – Eur. J.*, 2006, **12**, 1950; (*c*) C. Pichon, P. Mialane, A. Dolbecq, J. Marrot, E. Rivière, B. Keita, L. Nadjo and F. Sécheresse, *Inorg. Chem.*, 2007, **46**, 5292; (*d*) Z. Zhang, Y. Qi, C. Qin, Y. Li, E. Wang, X. Wang, Z. Su and L. Xu, *Inorg. Chem.*, 2007, **46**, 8162.

9 (*a*) S.-T. Zheng, D.-Q. Yuan, J. Zhang and G.-Y. Yang, *Inorg. Chem.*, 2007, **46**, 4569; (*b*) J. Zhao, H.-P. Jia, J. Zhang, S.-T. Zheng and G.-Y. Yang, *Chem. – Eur. J.*, 2007, **13**, 10030; (*c*) J.-W. Zhao, C.-M. Wang, J. Zhang, S.-T. Zheng and G.-Y. Yang, *Chem. – Eur. J.*, 2008, **14**, 9223; (*d*) B. Li, J.-W. Zhao, S.-T. Zheng and G.-Y. Yang, *Inorg. Chem.*, 2009, **48**, 8294; (*e*) W.-H. Fang, W.-D. Wang and G.-Y. Yang, *Dalton Trans.*, 2015, **44**, 12546.

10 G. Rousseau, O. Oms, A. Dolbecq, J. Marrot and P. Mialane, *Inorg. Chem.*, 2011, **50**, 7376.

11 O. Oms, S. Yang, W. Salomon, J. Marrot, A. Dolbecq, E. Rivière, A. Bonnefont, L. Ruhlmann and P. Mialane, *Inorg. Chem.*, 2016, **55**, 1551.

12 Z. Zhou, D. Zhang, L. Yang, P. Ma, Y. Si, U. Kortz, J. Niu and J. Wang, *Chem. Commun.*, 2013, **49**, 5189.

13 (*a*) L.-H. Bi and U. Kortz, *Inorg. Chem.*, 2004, **43**, 7961; (*b*) S. Nellutla, J. van Tol, N. S. Dalal, L.-H. Bi, U. Kortz, B. Keita, L. Nadjo, G. A. Khitrov and A. G. Marshall, *Inorg. Chem.*, 2005, **44**, 9795.

14 P. Mialane, A. Dolbecq, J. Marrot, E. Rivière and F. Sécheresse, *Angew. Chem., Int. Ed.*, 2003, **42**, 3523.

15 (*a*) S. S. Mal and U. Kortz, *Angew. Chem., Int. Ed.*, 2005, **44**, 3777; (*b*) S. S. Mal, B. S. Bassil, M. Ibrahim, S. Nellutla, J. van Tol, N. S. Dalal, J. A. Fernández, X. López, J. M. Poblet, R. Ngo Biboum, B. Keita and U. Kortz, *Inorg. Chem.*, 2009, **48**, 11636.

16 N. Laronze, J. Marrot and G. Hervé, *Inorg. Chem.*, 2003, **42**, 5857.

17 A. Tézé and G. Hervé, *Inorganic Syntheses*, John Wiley & Sons, New York, 1990, 27, 89.

18 *SAINT*, Bruker AXS Inc., Madison, WI, 2007.

19 (*a*) G. M. Sheldrick, *Acta Crystallogr., Sect. A: Found. Crystallogr.*, 2007, **64**, 112; (*b*) G. M. Sheldrick, *SADABS*, University of Göttingen, Göttingen, Germany, 1996.

20 G. M. Sheldrick, *SHELX, Program for Solution of Crystal Structures*, University of Göttingen, Göttingen, Germany, 2015.

21 (*a*) I. D. Brown, *Acta Crystallogr., Sect. B: Struct. Sci.*, 1992, **48**, 553; (*b*) I. D. Brown, *Acta Crystallogr., Sect. B: Struct. Sci.*, 1997, **53**, 381.

22 N. Laronze, J. Marrot and G. Hervé, *Chem. Commun.*, 2003, 2360.

23 S. G. Vulfson, *Molecular Magnetochemistry*, Gordon and Breach Science Publishers, 1998, p. 225.

24 (*a*) P. J. Kulesza, L. R. Faulkner, J. Chen and W. Klemperer, *J. Am. Chem. Soc.*, 1991, **113**, 379; (*b*) P. J. Kulesza and L. R. Faulkner, *J. Am. Chem. Soc.*, 1993, **115**, 11878; (*c*) M. Chojak, A. Kolary-Zurowska, R. Wlodarczyk, K. Miecznikowski, K. Karnicka, B. Palys, R. Marassi and P. J. Kulesza, *Electrochim. Acta*, 2007, **52**, 5574; (*d*) I. A. Rutkowska and P. J. Kulesza, in *Encyclopedia of Interfacial Chemistry: Surface Science and Electrochemistry*, ed. K. Wandelt, Elsevier, 2018, vol. 5, p. 207; (*e*) M. H. Dickman, T. Ozeki, H. T. Evans Jr., C. Rong, G. B. Jameson and M. T. Pope, *J. Chem. Soc., Dalton Trans.*, 2000, 149–154.

25 A. J. Bard and L. R. Faulkner, *Electrochemical Methods*, VCH, New York, 1994.

26 (*a*) Y. Hori, I. Takahashi, O. Koga and N. Hoshi, *J. Phys. Chem. B*, 2002, **106**, 15; (*b*) Y. Hori, I. Takahashi, O. Koga and N. Hoshi, *J. Mol. Catal. A: Chem.*, 2003, **199**, 39; (*c*) N. Hoshi, E. Sato and Y. Hori, *J. Electroanal. Chem.*, 2003, **540**, 105; (*d*) A. A. Peterson, F. Abild-Pedersen, F. Studt, J. Prossmeisl and J. K. Nørskov, *Energy Environ. Sci.*, 2010, **3**, 1311; (*e*) O. A. Baturina, Q. Lu, M. A. Padila, L. Xin, W. Li, A. Serov, K. Artyushkova, P. Atanassov, F. Xu, A. Epshteyn, T. Brintlinger, M. Schuette and G. E. Collins, *ACS Catal.*, 2014, **4**, 3682.

27 B. Keita, E. Abdeljalil, L. Nadjo, R. Contant and R. Belgiche, *Langmuir*, 2006, **22**, 10416.

28 A. Wadas, I. A. Rutkowska, M. Bartel, S. Zoladek, K. Rajeshwar and P. J. Kulesza, *Russ. J. Electrochem.*, 2017, **53**, 1194.

29 (*a*) H. Ooka, M. C. Figueiredo and M. T. M. Koper, *Langmuir*, 2017, **33**, 9307; (*b*) P. J. Kulesza, I. A. Rutkowska and A. Wadas, in *Encyclopedia of Interfacial Chemistry: Surface Science and Electrochemistry*, ed. K. Wandelt, Elsevier, 2018, vol. 5, p. 521; (*c*) J. Qiao, Y. Liu, F. Hong, F. Hong and J. Zhang, *Chem. Soc. Rev.*, 2014, **43**, 631; (*d*) K. P. Kuhl, E. R. Cave, D. N. Abram and T. F. Jaramillo, *Energy Environ. Sci.*, 2012, **5**, 7050; (*e*) C. H. Lee and M. W. Kanan, *ACS Catal.*, 2015, **5**, 465.

30 (*a*) P. Dube and G. M. Brisard, *J. Electroanal. Chem.*, 2005, **582**, 230; (*b*) Y. Hori, A. Murata and R. Takahashi, *J. Chem. Soc., Faraday Trans. 1*, 1989, **85**, 2309; (*c*) M. Lee, M. Ren, Z. Zhang, P. T. Sprunger, R. L. Kurtz and J. C. Flake, *J. Electrochem. Soc.*, 2011, **158**, E45.

31 Y. Lan, S. Ma, J. Lu and P. J. A. Kenis, *Int. J. Electrochem. Sci.*, 2014, **9**, 7300.

32 (*a*) J. Krzystek, S. A. Zvyagin, A. Ozarowski, S. Trofimenko and J. Telser, *J. Magn. Reson.*, 2006, **178**, 174; (*b*) J. H. Christian, D. W. Brogden, J. K. Bindra, J. S. Kinyon, J. van Tol, J. Wang, J. F. Berry and N. S. Dalal, *Inorg. Chem.*, 2016, **55**, 6377.

33 C. S. Le Duff, M. J. Lawrence and P. Rodriguez, *Angew. Chem., Int. Ed.*, 2017, **56**, 12919.

34 (*a*) K. W. Frese Jr., *Electrochemical and Electrocatalytic Reactions of Carbon Dioxide*, Elsevier, Amsterdam, 1993; (*b*) Y. Momose, K. Sato and O. Ohno, *Surf. Interface Anal.*, 2002, **34**, 615; (*c*) H. Shibata, J. A. Moulijn and G. Mul, *Catal. Lett.*, 2008, **123**, 186; (*d*) Ch. W. Li and M. W. Kanan, *J. Am. Chem. Soc.*, 2012, **134**, 7231; (*e*) W. Tang, A. A. Peterson, A. S. Varela, Z. P. Jovanov, L. Bech, W. J. Durand, S. Dahl, J. K. Norskov and I. Chorkendorff, *Phys. Chem. Chem. Phys.*, 2012, **14**, 76; (*f*) M. R. Goncalves, A. Gomes, J. Condeco, T. R. C. Fernandes, T. Pardal, C. A. C. Sequeira and J. B. Branco, *Electrochim. Acta*, 2013, **102**, 388.

35 (*a*) M. Goral, M. Jouini, C. Perruchot, K. Miecznikowski, I. A. Rutkowska and P. J. Kulesza, *Electrochim. Acta*, 2011, **56**, 3605; (*b*) D. Szymanska, I. A. Rutkowska, L. Adamczyk, S. Zoladek and P. J. Kulesza, *J. Solid State Electrochem.*, 2010, **14**, 2049.

36 E. Szaniawska, I. A. Rutkowska, M. Frik, A. Wadas, E. Seta, A. Krogul-Sobczak, K. Rajeshwar and P. J. Kulesza, *Electrochim. Acta*, 2018, **265**, 400.